International Journal of Thermophysics, Vol. 21, No. 4, 2000

Thermophysical Properties of Gaseous HBr and BCl_3 from Speed-of-Sound Measurements

J. J. Hurly[1]

Received December 22, 1999

The speed of sound in gaseous hydrogen bromide (HBr) and boron trichloride (BCl_3) was measured using a highly precise acoustic resonance technique. The HBr speed-of-sound measurements span the temperature range 230 to 440 K and the pressure range from 0.05 to 1.5 MPa. The BCl_3 speed-of-sound measurements span the temperature range 290 to 460 K and the pressure range from 0.05 MPa to 0.40 MPa. The pressure range in each fluid was limited to 80% of the sample vapor pressure at each temperature. The speed-of-sound data have a relative standard uncertainty of 0.01%. The data were analyzed to obtain the ideal-gas heat capacities as a function of temperature with a relative standard uncertainty of 0.1%. The heat capacities agree with those calculated from spectroscopic data within their combined uncertainties. The speeds of sound were fitted with the virial equation of state to obtain the temperature-dependent density virial coefficients. Two virial coefficient models were employed, one based on the hard-core square-well intermolecular potential model and the second based on the hard-core Lennard–Jones intermolecular potential model. The resulting virial equations of state reproduced the speed-of-sound measurements to 0.01% and can be expected to calculate vapor densities with a relative standard uncertainty of 0.1%. Transport properties calculated from the hard-core Lennard–Jones potential model should have a relative standard uncertainty of 10% or less.

KEY WORDS: BCl_3; boron trichloride; equation of state; HBr; hydrogen bromide; speed of sound; thermodynamic properties; transport properties; virial coefficients.

1. INTRODUCTION

Many reactive, corrosive, and toxic compounds are used in the processing of semiconductors. The properties which make these compounds useful also

[1] Physical and Chemical Properties Division, Chemical Science and Technology Laboratory, National Institute of Standards and Technology, Gaithersburg, Maryland 20899-8380, U.S.A.

0195-928X/00/0700-0805$18.00/0

make them difficult to study. Issues such as material compatibility, sample purity, and environmental and personnel safety must be considered. Our laboratory is using acoustic techniques to measure the thermophysical properties of these compounds in the gaseous state. These properties are used in process design, in purification of the process gases, and for accurate calibration of mass flow controllers (MFCs) used throughout the semiconductor industry. The actual calibration of the MFCs is performed with nonhazardous surrogate gases, and then a "correction" factor is employed to scale the actual metering of the hazardous or reactive species. To determine accurate "correction" factors from physical models, one requires the equation of state $P(V, T)$, the ideal-gas heat capacity, $C_p^\circ(T)$, the thermal conductivity, κ, and the viscosity, λ.

Here, we report on measured speed-of-sound data $u(T, P)$ in hydrogen bromide (HBr) and boron trichloride (BCl_3). The data are used to deduce the vapor-phase equation of state and the ideal-gas heat capacity and, also, to estimate the transport properties. Subsequent publications from our laboratory will report direct measurements of the transport properties.

2. APPARATUS AND PROCEDURES

The apparatus employed here has been described in detail elsewhere [1, 2]. The original version of the apparatus was used to study successfully more than 20 nonhazardous gases and gas mixtures. The modifications for handling reactive and hazardous gases are described in Ref. 3. The model for the acoustic resonator is described in Refs. 4 and 5. A detailed description of the experimental procedures can be found in Refs. 3 and 6.

The gas samples were obtained from commercial suppliers. The HBr was V.L.S.I. (very large scale integration) grade certified to 99.995% by volume, and the BCl_3 was classified as etchant grade certified to 99.99% by volume. For both fluids, sample was taken from the liquid phase and no appreciable overpressure was observed when the sample was collected in a liquid nitrogen trap at 77 K.

3. RESULTS

The thermodynamic states studied for each fluid are shown in Fig. 1. An open circle represents each state where a speed-of-sound measurement was recorded. Figure 1 also shows the vapor pressure curve [7] and the critical point [8, 9] for each fluid. At each temperature and pressure, the resonance frequencies of two longitudinal and one radial mode were recorded and used to compute the speed of sound. The mean of these three values of the speed of sound and their relative standard uncertainty with

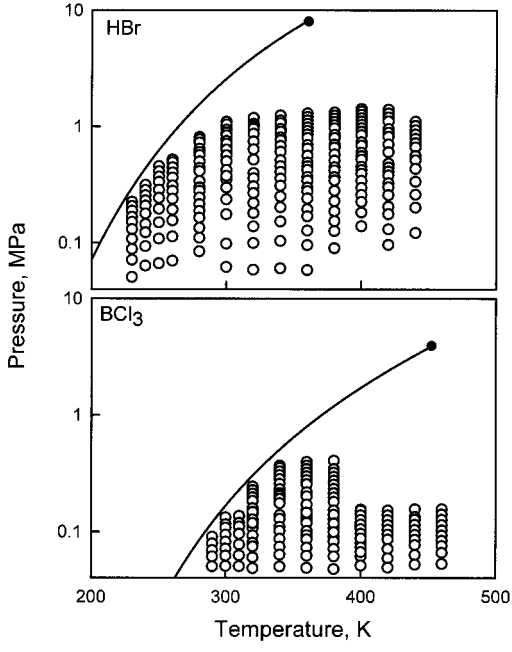

Fig. 1. Phase diagram for HBr (top) and BCl_3 (bottom) with the vapor pressure curves [7] ending at the critical point [8, 9] for each fluid. The state points at which speed-of-sound measurements were made are shown as open circles.

a coverage factor $k = 2$ are tabulated in Table I for HBr and in Table II for BCl_3.

The speed of sound in HBr was measured at 232 state points, along 13 isotherms, spanning the temperature range 230 to 440 K and the pressure range 0.05 to 1.5 MPa. Pressures were limited to 80% of the sample vapor pressure at a given temperature. The 300 K isotherm was repeated to demonstrate reproducibility.

The BCl_3 measurements were made at 167 state points, along 17 isotherms spanning the temperature range of 290 to 440 K and the pressure range 0.05 to 0.4 MPa. Pressures were limited to 80% of the sample vapor pressure at a given temperature. As discussed below, we experienced difficulty obtaining reproducible results in BCl_3 when we attempted measurements above 0.15 MPa, the room-temperature vapor pressure of BCl_3. Initially, a series of measurements was recorded with the resonator loaded to approximately 0.15 MPa. A fresh sample from the liquid phase was withdrawn from the manufacture's container and used for each isotherm.

Table I. Measured Sound Speeds in Hydrogen Bromide

P (kPa)	u ($m \cdot s^{-1}$)	$10^6\sigma[u]/u$
	$T = 230$ K	
225.0	177.659	62
207.2	178.030	44
188.5	178.397	48
167.0	178.819	47
151.7	179.114	55
131.3	179.503	83
108.1	179.929	22
88.7	180.295	57
71.5	180.609	39
51.0	180.976	18
	$T = 240$ K	
314.3	180.582	57
284.1	181.120	58
256.4	181.603	44
231.5	182.036	56
208.8	182.423	41
178.8	182.930	60
145.1	183.488	48
123.1	183.850	62
93.6	184.329	63
63.8	184.800	39
	$T = 250$ K	
455.9	182.796	49
411.4	183.522	64
370.9	184.170	57
334.2	184.745	50
285.2	185.494	48
243.4	186.128	50
196.5	186.831	50
150.2	187.505	47
108.7	188.100	26
66.8	188.692	41
	$T = 260$ K	
518.5	186.464	49
492.9	186.832	70
445.5	187.510	63
402.2	188.118	39
363.2	188.658	63
310.5	189.375	28
279.8	189.785	40
239.1	190.329	56
193.3	190.929	27
156.3	191.402	46
113.6	191.954	49
70.5	192.494	54
	$T = 280.00$ K	
812.6	191.834	77
774.0	192.298	77
727.2	192.848	77
642.6	193.835	65
603.8	194.274	73
567.5	194.685	67
500.1	195.439	62
440.8	196.087	65
413.1	196.394	54
340.6	197.170	63
298.6	197.619	56
279.6	197.817	54
244.8	198.181	54
214.8	198.491	49
188.0	198.772	47
164.9	199.011	53
135.0	199.317	44
110.8	199.567	50
84.7	199.834	61
	$T = 300$ K	
1001.7	198.848	75
947.3	199.372	70
939.8	199.445	68
883.5	199.978	67
789.5	200.859	72
745.7	201.265	64
665.3	201.999	65
627.9	202.337	67
559.6	202.951	63
418.3	204.193	58
350.9	204.777	61
	$T = 300.00$ K	
1099.1	197.903	89
1040.1	198.486	76
939.8	199.454	68
888.0	199.947	72
839.6	200.401	74
750.3	201.232	69
710.3	201.599	66
633.4	202.299	62
564.6	202.916	60
503.0	203.462	61
423.0	204.164	58
376.8	204.565	62
299.1	205.231	55
236.5	205.762	55
176.5	206.265	48
98.6	206.913	25
62.2	207.210	88
	$T = 320$ K	
1187.7	205.888	82
1054.4	206.920	42
1006.6	207.290	65
958.7	207.653	75
866.8	208.345	74
744.5	209.256	69
637.5	210.042	63
519.3	210.896	61
398.1	211.758	48
358.4	212.037	59
306.5	212.400	54
268.5	212.668	66
220.2	213.004	69
180.7	213.277	54
139.0	213.563	39
100.0	213.827	25
58.9	214.108	114
	$T = 340$ K	
1250.1	213.645	99
1127.7	214.422	66
1128.0	214.421	78
1068.0	214.794	77
955.5	215.491	72
903.3	215.809	73
806.1	216.398	72

Table I. *(Continued)*

P (kPa)	u ($m \cdot s^{-1}$)	$10^6\sigma[u]/u$	P (kPa)	u ($m \cdot s^{-1}$)	$10^6\sigma[u]/u$	P (kPa)	u ($m \cdot s^{-1}$)	$10^6\sigma[u]/u$
	$T = 230$ K		1245.9	228.5	64	298.2	238.689	53
762.8	216.662	68	1169.3	228.9	64	259.2	238.821	45
680.4	217.158	68	1095.9	229.2	53	225.9	238.935	42
607.5	217.592	61	1028.8	229.5	53	183.3	239.082	39
512.5	218.153	58	967.0	229.7	55	139.6	239.233	76
456.2	218.485	54	850.8	230.2	60			
407.3	218.773	59	797.6	230.4	48		$T = 420$ K	
357.1	219.067	51	701.5	230.8	55	1402.5	241.490	52
310.2	219.337	54	659.2	231.0	53	1298.8	241.798	56
250.7	219.684	48	578.4	231.3	25	1202.6	242.083	53
202.8	219.958	56	509.5	231.6	52	1113.5	242.344	48
153.0	220.242	71	447.4	231.9	54	955.4	242.807	43
104.2	220.517	53	419.6	232.0	55	885.3	243.014	45
60.6	220.765	39	367.8	232.2	47	820.0	243.207	48
			344.6	232.3	56	704.0	243.546	48
	$T = 360$ K		281.3	232.6	53	603.9	243.839	48
1300.9	221.061	81	229.7	232.8	43	480.9	244.199	51
1213.0	221.514	66	229.7	232.8	41	444.8	244.304	48
1131.5	221.929	63	188.0	232.9	43	411.8	244.402	46
1055.1	222.317	63	154.2	233.1	47	381.1	244.491	40
983.6	222.679	59	126.7	233.2	47	326.4	244.653	48
916.9	223.016	58	90.4	233.3	107	302.0	244.723	42
855.1	223.326	67				258.4	244.851	65
798.2	223.611	61				205.5	245.003	36
694.6	224.124	60		$T = 400$ K		177.2	245.089	32
647.8	224.357	58	1421.7	234.757	64	131.4	245.227	46
563.5	224.773	56	1349.3	235.015	57	96.6	245.332	68
489.2	225.138	52	1264.1	235.315	52			
455.8	225.299	57	1184.0	235.596	50		$T = 440$ K	
424.7	225.453	53	1108.7	235.861	51	1105.4	248.553	66
369.1	225.724	56	1037.1	236.113	49	1016.0	248.775	60
343.7	225.846	54	969.1	236.353	52	933.8	248.977	56
298.6	226.065	58	904.9	236.577	54	856.4	249.169	51
278.2	226.163	51	844.8	236.787	53	786.9	249.341	49
241.3	226.341	47	734.8	237.172	50	722.2	249.502	51
195.2	226.565	57	686.0	237.341	57	663.2	249.649	52
169.5	226.684	42	596.9	237.650	53	560.8	249.902	52
127.7	226.885	49	556.8	237.790	47	514.9	250.017	52
96.2	227.039	70	520.1	237.917	50	434.7	250.216	53
58.6	227.217	62	452.2	238.152	44	337.0	250.458	42
			422.5	238.255	43	260.6	250.649	40
	$T = 380$ K		394.3	238.353	45	202.1	250.795	41
1325.4	228.2	69	342.6	238.532	49	122.4	250.988	41

Table II. Measured Sound Speeds in Boron Trichloride

P (kPa)	u ($m \cdot s^{-1}$)	$10^6\sigma[u]/u$
	$T = 290$ K	
90.1	150.724	32
79.0	151.175	41
69.3	151.568	32
61.1	151.891	59
50.2	152.314	71
	$T = 300$ K	
132.4	151.958	26
115.5	152.605	33
107.9	152.890	17
94.0	153.407	32
81.8	153.851	33
71.3	154.229	39
62.1	154.553	17
50.6	154.956	17
	$T = 310$ K	
136.2	154.716	31
118.4	155.325	23
110.2	155.600	32
95.7	156.085	18
77.3	156.692	36
62.4	157.178	33
50.3	157.564	21
	$T = 320$ K	
150.7	157.049	32
140.3	157.379	43
123.7	157.895	42
115.1	158.162	46
107.0	158.408	54
92.5	158.850	55
80.0	159.227	41
74.4	159.393	14
59.9	159.821	13
48.3	160.162	10
	$T = 340$ K	
138.6	162.803	43
128.3	163.075	41
109.7	163.557	39
101.4	163.769	29
86.6	163.145	29
74.1	164.459	49
63.4	164.724	20
50.1	165.059	25
	$T = 360$ K	
151.9	167.603	40
140.1	167.866	46
129.2	168.109	41
119.1	168.332	30
101.1	168.727	49
93.1	168.902	58
85.8	169.056	33
72.8	169.336	75
62.1	169.560	16
48.7	169.846	16
	$T = 380$ K	
152.2	172.531	45
139.6	172.769	46
127.8	172.992	40
117.2	173.194	36
107.3	173.377	33
90.1	173.700	24
82.6	173.843	55
71.2	174.053	54
61.3	174.234	45
47.6	174.485	23
	$T = 400$ K	
155.1	177.214	16
141.6	177.437	44
127.4	177.673	41
121.3	177.773	43
109.1	177.972	34
96.1	178.182	44
80.2	178.440	42
73.2	178.550	26
61.4	178.739	10
51.1	178.904	14
	$T = 400$ K	
151.6	177.284	31
151.5	177.283	32
151.4	177.283	38
151.3	177.283	42
151.5	177.283	33
151.5	177.283	31
151.6	177.281	30
151.5	177.283	37
151.6	177.283	28
151.5	177.282	31
151.5	177.283	31
151.2	177.501	39
151.1	177.697	35
151.1	177.877	38
151.1	178.040	27
151.9	178.188	35
151.6	178.324	44
151.1	178.557	41
151.8	178.659	33
151.2	178.907	35
	$T = 420.00$ K	
152.0	181.847	42
138.3	182.042	39
125.8	182.224	41
114.4	182.387	56
103.9	182.532	44
94.4	182.669	42
85.9	182.786	26
71.2	182.991	30
59.1	183.165	49
49.1	183.304	67
	$T = 440.00$ K	
155.7	186.236	27
134.0	186.507	19
126.6	186.597	12

Table II. *(Continued)*

P (kPa)	u ($m \cdot s^{-1}$)	$10^6\sigma[u]/u$	P (kPa)	u ($m \cdot s^{-1}$)	$10^6\sigma[u]/u$	P (kPa)	u ($m \cdot s^{-1}$)	$10^6\sigma[u]/u$
114.6	186.750	30	158.4	156.790	42	345.3	163.113	10
103.7	186.887	37	147.3	157.137	36	320.7	163.700	16
94.0	187.008	22	127.3	157.761	41	298.3	164.227	12
85.1	187.115	41	118.3	158.039	40	276.4	164.742	14
76.8	187.221	31				255.2	165.232	21
63.2	187.387	20		$T = 340.00$ K[a]		217.4	166.099	27
52.2	187.526	54		($f_c = 1.000347$)		200.6	166.477	31
			369.4	156.388	72	170.7	167.149	30
	$T = 460.00$ K		352.6	156.877	14	145.2	167.716	33
156.0	190.542	27	328.4	157.575	11			
140.5	190.714	23	305.5	158.229	12		$T = 380.00$ K[a]	
126.6	190.873	45	281.6	158.902	13		($f_c = 1.000198$)	
114.1	191.008	31	257.2	159.582	16	145.2	167.716	33
102.9	191.136	62	231.1	160.301	22	406.9	167.457	15
92.8	191.244	35	213.6	160.776	28	345.2	168.708	14
83.7	191.349	42	210.6	160.858	26	320.0	169.212	15
75.5	191.434	50	201.1	161.114	26	295.8	169.693	13
66.0	191.542	33	201.2	161.110	27	274.1	170.121	18
52.9	191.683	18	201.7	161.097	26	252.9	170.535	27
			189.9	161.414	30	232.5	170.934	27
	$T = 320.00$ K[a]		175.2	161.809	28	213.6	171.300	30
	($f_c = 1.000155$)					196.2	171.635	36
243.5	154.017	16		$T = 360.00$ K[a]		180.2	171.941	32
226.7	154.577	17		($f_c = 1.000217$)		151.8	172.482	46
211.3	155.087	25				139.4	172.717	40
196.7	155.561	28	396.7	161.868	10	117.5	173.131	43
183.1	156.003	34	368.3	162.559	18	99.0	173.474	35

[a] We recommend multiplying the values of u on these isotherms by f_c.

The 400 K isotherm was repeated to test the reproducibility of this loading technique. Furthermore, at 400 K and 0.15 MPa, the speed of sound was monitored for 6 h, the same time period required to complete measurements along each isotherm. The speed of sound did not vary outside the experimental uncertainties during this period, showing that the sample composition did not change once it was loaded into the resonator. A second series of measurements at pressures above 0.15 MPa was attempted. For these, a portion of liquid BCl_3 was transferred into a small stainless steel cylinder connected to the heated gas manifold. The small cylinder was

gently heated in a beaker of warm water to supply gas at pressures above 0.15 MPa. The speed of sound in the gas loaded by this technique was 0.01 to 0.03% lower than that in the samples loaded directly from the manufacturer's container. This change in the speed of sound was attributed to a reaction of some of the BCl_3, which changed the mean molecular weight of the sample (m). The ideal-gas speed of sound u_o is related to the mean molecular weight through $u_o^2 = \gamma^0 RT/m$, where $\gamma^0 = (C_p^o/C_v^o)$ is the ratio of the ideal-gas heat capacities, R is the gas constant, T is the temperature, and m is the mean molecular weight of the sample gas.

Once the resonator was loaded, no further speed-of-sound changes occurred. This indicated that the composition change occurred either in the heated stainless-steel volume or in the heated gas manifold. In any case, we obtained useful results at pressures up to 0.4 MPa along four isotherms; 320, 340, 360, and 380 K.

4. IDEAL-GAS HEAT CAPACITY

The speed-of-sound measurements were recorded along isotherms. The data on each isotherm were fitted by the acoustic virial equation of state:

$$u^2 = \frac{\gamma^0 RT}{m}\left(1 + \frac{\beta_a P}{RT} + \frac{\gamma_a P^2}{RT} + \frac{\delta_a P^3}{RT} + \cdots\right) \tag{1}$$

where T is the temperature (ITS-90), and β_a, γ_a, and δ_a are the temperature-dependent acoustic virial coefficients. On each isotherm $C_p^o(T)$ is obtained from the zero-pressure intercept of Eq. (1) through the relation $C_p^o(T)/R = \gamma^0/(\gamma^0 - 1)$ The resulting values of $C_p^o(T)/R$ for each species are reported in Table III.

The results of HBr and BCl_3 provide contrasting examples of a well-behaved fluid and a difficult fluid. The HBr data are an example of the best results that this apparatus can provide. Isotherms proved reproducible under all conditions. HBr has an adequate vapor pressure at room temperature. Data analysis occurred without any problems. The BCl_3 data are a good example of what problems our apparatus can encounter. The room-temperature vapor pressure of BCl_3 is only 0.15 MPa. All attempts to achieve higher pressures by gently heating an isolated BCl_3 sample resulted in irreproducible results. This limited the pressure range of the data. However, even with these difficulties, the equation of state determined for BCl_3 is still expected to predict gas densities to better than 0.1%.

Table III. Ideal-Gas Heat Capacities $C_p^\circ(T)/R$ Determined for Each Isotherm

HBr		BCl_3	
T (K)	$C_p^\circ(T)/R$	T (K)	$C_p^\circ(T)/R$
230	3.5024	290	7.4514
240	3.5020	300	7.5407
250	3.5028	310	7.6076
260	3.5033	320	7.6906
280	3.5033	340	7.8380
300	3.5040	360	8.0010
300	3.5034	380	8.1249
320	3.5045	400	8.2464
340	3.5052	400	8.2462
360	3.5062	420	8.3644
380	3.5093	440	8.4610
400	3.5132	460	8.5480
420	3.5145		
440	3.5210		

4.1. Hydrogen Bromide

Hydrogen bromide is a simple diatomic with a single low-lying vibrational mode accessible at these temperatures. This allows for a very accurate calculation of the ideal-gas heat capacity from statistical mechanics. Accepting the accuracy of the estimated C_p° values, we can consider our measurement of C_p° for HBr to be a test of our experimental technique. The C_p°/R values for HBr reported in Table III were fitted with the expression derived from statistical mechanics for the ideal-gas heat capacity. We assumed that (a) the electronic contributions to the heat capacity are negligible, (b) the translational $C_{p,t}^\circ/R$ and rotational $C_{p,v}^\circ/R$ contributions are independent of temperature, and (c) the vibrational contribution has the Einstein form. Thus we fitted the data to

$$\frac{C_p^\circ}{R} = \frac{C_{p,t}^\circ + C_{p,v}^\circ}{R} + \frac{(\Theta T)^2 e^{(\Theta/T)}}{(e^{(\Theta/T)} - 1)^2} \tag{2}$$

The fit yielded $C_{p,t}^\circ + C_{p,v}^\circ = (3.5026 \pm 0.006)\, R$ and the characteristic vibrational temperature $\Theta = 3626.7 \pm 68.9$ K. The fit has a relative standard uncertainty of 0.014%. We expected $C_{p,t}^\circ + C_{p,r}^\circ = 3.5$. The small difference between 3.5 and 3.5026 is consistent with our estimates that the relative standard uncertainty of C_p°/R is 0.1%. The value $\Theta = 3667.3$ K from spectroscopy [10] agrees with the results of the fit within estimated uncertainties.

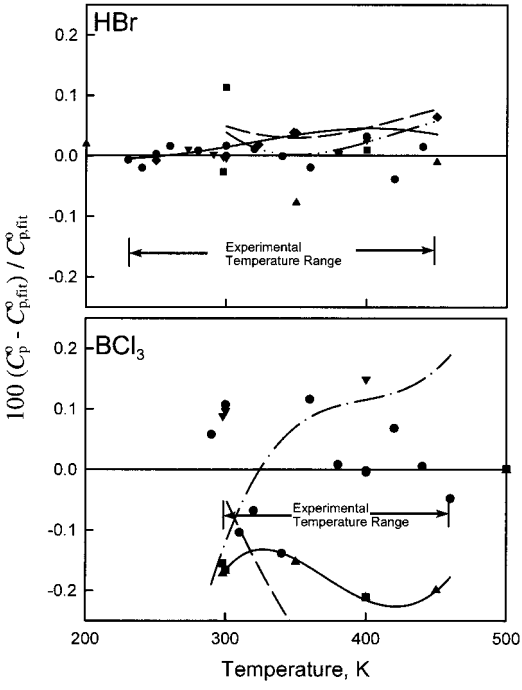

Fig. 2. Percentage deviations of ideal-gas heat capacity from Eq. (2). Top (HBr): (——) correlation, Ref. 34; (- - - - -) correlation, Ref. 35; (– · – ·) correlation, Ref. 36; (●) present work; (□) Ref. 37; (△) Ref. 38; (▽) Ref. 39; (◇) Ref. 40. Bottom (BCl_3): Curves are same as top; (●) present work; (□) Ref. 31; (△) Ref. 41; (▽) Ref. 42; (◇) Ref. 43; (⬡) Ref. 44.

Figure 2 shows that the values of C°_{p} reported in Table III are within our claimed uncertainty of 0.1 % of the values calculated from spectroscopy.

4.2. Boron Trichloride

Boron trichloride is a more complicated molecule than HBr. BCl_3 is a planar molecule with a D_{3h} symmetry. Consequently, the calculation of its ideal-gas heat capacity is more difficult than that of HBr and Eq. (2) cannot be used to fit the data. Consequently, the BCl_3 data in Table III are fitted by the polynomial

$$C^{\circ}_{p}(T)/R = 3.85517 + 0.0160967T - 1.279545 \times 10^{-5}T^{2} \qquad (3)$$

with a relative standard uncertainty of 0.061 %. Equation (3) is valid only in the temperature range spanned by the data. Figure 2 shows the deviations of the values of C_p°/R listed in Table III from those calculated by Eq. (3). Calculated and estimated values of C_p°/R obtained from the literature are also shown in Fig. 2, along with previous correlations of these estimates. Slight changes in the composition of the BCl_3 are suggested by the scatter about Eq. (3). However, the reported values are still nearly all within 0.1 % of Eq. (3).

5. VIRIAL EQUATION OF STATE

In Section 4 we determined C_p°/R from the zero-pressure intercepts of each isotherm. From the slope, du^2/dP, of each isotherm we can obtain some information about the equation of state. By considering the entire $u^2(T, P)$ surface and by making reasonable assumptions we can deduce a virial equation of state for the vapor phase of each fluid. The virial equation of state is given by

$$P = RT\rho[1 + B(T)\,\rho + C(T)\,\rho^2 + \cdots] \tag{4}$$

where P is pressure, ρ is density, and $B(T)$ and $C(T)$ are the second and third density virial coefficients. The acoustic virial coefficients in Eq. (1) are directly related to the density virial coefficients in Eq. (4) through exact thermodynamic equations involving the density virial coefficients, their temperature derivatives, and $\gamma^0(T)$. These equations appear in Ref. 11 and allow us to determine parameters in models for $B(T)$ and $C(T)$ from the $u^2(T, P)$ surface.

Inverse temperature polynomials are often used to model the temperature dependences of the virial coefficients. This representation is a valid approximation only when the reduced temperature $T_r = T/T_c \gg 1$, where T_c is the critical temperature. This model extrapolates poorly and is inappropriate in our experimental temperature ranges where $T_r < 1$. A more useful representation of the virial coefficients can be obtained from a model of intermolecular interactions or the intermolecular potential function. Here we use two such models: (1) the hard-core square-well (HCSW) model and (2) the hard-core Lennard–Jones (HCLJ) model.

5.1. The Hard-Core Square-Well Potential Model (HCSW)

The HCSW model of molecular interactions has an intermolecular potential function φ of the form

$$\begin{aligned} &= \infty, && r < \sigma \\ \varphi(r) &= \varepsilon, && \sigma \leqslant r \leqslant \sigma\lambda \\ &= 0, && r > \sigma\lambda \end{aligned} \tag{5}$$

and is shown in Fig. 3. This simple representation of intermolecular interactions has the advantage that the integrals [Eqs. (11) and (12) below] required to compute the second and third virial coefficients lead to algebraic functions in temperature [11]. These functions expressing $B(T)$ and $C(T)$ in terms of the HCSW potential parameters are

$$B(T) = b_o[1 - (\lambda^3 - 1)\,\Delta] \tag{6}$$

$$\begin{aligned} C(T) &= \tfrac{1}{8} b_o^2 (5 - c_1\Delta - c_2\Delta^2 - c_3\Delta^3) \\ c_1 &= \lambda^6 - 18\lambda^4 + 32\lambda^3 - 15 \\ c_2 &= 2\lambda^6 - 36\lambda^4 + 32\lambda^3 + 18\lambda^2 - 16 \\ c_3 &= 6\lambda^6 - 18\lambda^4 + 18\lambda^2 - 6 \end{aligned} \tag{7}$$

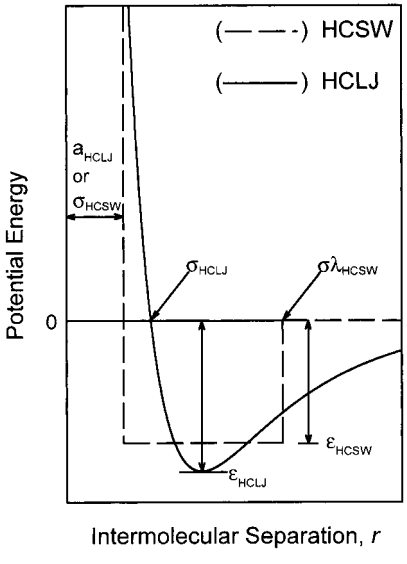

Fig. 3. Hard-core square-well and hard-core Lennard–Jones intermolecular potential models.

where $\Delta = e^{\varepsilon/k_B T} - 1$, and k_B is Boltzmann's constant. The adjustable parameters are ε, the well depth; σ, the hard-core diameter; and λ, the ratio of the width of the well to σ. Here b_o is the molar volume of the hard core $b_o = \frac{2}{3}\pi N_A \sigma^3$, and N_A is Avogadro's constant. Equations (6) and (7) allow the virial coefficients and their temperature derivatives to be calculated explicitly at a given temperature. This allows the $u^2(T, P)$ surface to be fitted directly to Eq. (4).

Gillis and Moldover [11] have shown that Eqs. (6) and (7) do an excellent job at fitting speed-of-sound measurements. The HCSW expressions for $B(T)$ and $C(T)$ have realistic temperature dependences that extrapolate to reasonable values, and the densities computed from these virial coefficients have small uncertainties in a useful range of conditions [11]. We follow Ref. 11 in using different values of b_o, ε, and λ for $B(T)$ and $C(T)$; thus, this model has six parameters. This is because we are using Eqs. (6) and (7) only for their physical form and asymptotic behavior, not actually to determine the potential parameters.

5.1.1. The HCSW Model for HBr

The 230 speed-of-sound measurements in HBr extended to pressures of 1.5 MPa. The $u^2(T, P)$ data in this range required both the second and the third virial coefficients to be modeled properly. The ideal-gas heat capacity was held fixed at that given by Eq. (2). The six parameters, three for $B(T)$ and three for $C(T)$, were allowed to vary. The resulting parameters are provided in Table IV. Figure 4 (top) shows the deviations of the measured speeds of sound in HBr from those calculated from fitting the HCSW virial equation of state. The measured speeds of sound are reproduced with a relative standard deviation of $\pm 0.004\%$. The fit had 223 degrees of freedom v, and χ^2/v was 0.74, where $\chi^2 = \sum_i [f(x_i) - f_i]^2/\sigma_f^2$, and $f(x_i) = u^2(P, T)$.

Table IV. Parameters for HCSW Equations of State Deduced from $u^2(T, P)$ Measurements

	b_o ($m^3 \cdot mol^{-1}$)	λ	ε/k_B (K)
	HBr		
$B(T)$ ($cm^3 \cdot mol^{-1}$)	4.0854×10^{-5}	1.4549	385.22
$C(T)$ ($cm^3 \cdot mol^{-1}$)^2	9.9251×10^{-5}	1.2277	414.45
	BCl_3		
$B(T)$ ($cm^3 \cdot mol^{-1}$)	1.5065×10^{-4}	1.4909	373.59
$C(T)$ ($cm^3 \cdot mol^{-1}$)^2	2.1283×10^{-4}	1.3601	455.32

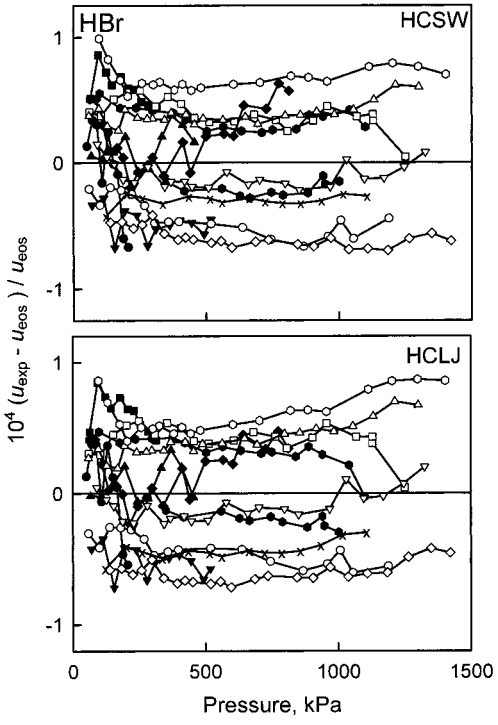

Fig. 4. Fractional deviations of HBr speed-of-sound data from that predicted by our equations of state. Top: HCSW equation of state. Bottom: HCLJ equation of state. (●) 230 K; (■) 240 K; (▲) 250 K; (▼) 260 K; (◆) 280 K; (○) 300 K; (□) 320 K; (△) 340 K; (▽) 360 K; (◇) 380 K; (⬢) 400 K; (✖) 420 K; (✚) 440 K.

5.1.2. The HCSW Model for BCl_3

The sound-speed measurements in BCl_3 extended only to 0.4 MPa with the data collected in two stages. Measurements up to 0.15 MPa were collected first, and then isotherms at 320, 340, 360, and 380 K were extended to 0.4 MPa. In Section 3 we discussed how a slight change in the average molecular weight was observed in the four higher-pressure isotherms. To compensate for this change in average molecular weight, the speeds of sound along each isotherm were multiplied by a constant (f_c) chosen to shift each high-pressure isotherm so that it overlapped the corresponding low-pressure isotherm. The values of f_c are given in Table II.

It is recommended that the correction be applied to the four high-pressure isotherms reported in Table II before their use. The initial series of low pressure isotherms, with the exception of the 290 and 300 K isotherms, required only the second virial coefficient to be fitted by Eq. (4). The inclusion of the four higher pressure isotherms necessitated the inclusion of $C(T)$ and reduced the overall quality of the fit. The resulting parameters are provided in Table IV. The fit had $v = 160$ and a χ^2/v of 2.63. Figure 5 (top) shows the deviations of the adjusted $u(T, P)$ values from that calculated from the determined equation of state. The equation of state reproduced the adjusted sound speeds with a standard relative deviation of 0.003%.

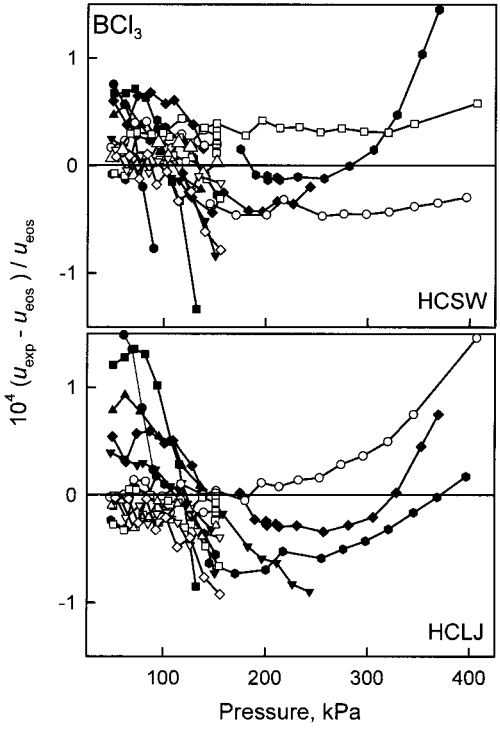

Fig. 5. Fractional deviations of BCl_3 speed-of-sound data from that predicted by our equations of state. Top: HCSW equation of state. Bottom: HCLJ equation of state. (●) 290 K; (■) 300 K; (▲) 310 K; (▼) 320 K; (◆) 340 K; (⬢) 360 K; (○) 380 K; (□) 400 K; (△) 420 K; (▽) 440 K; (◇) 460 K; (⬡) 440 K.

5.2. Analysis with the HCLJ Potential Model

The HCLJ analysis is similar to the HCSW analysis; however, it was more difficult to implement. The hard-core Lennard–Jones (6)–(12) potential [12] is

$$\varphi(r_{ij}) = 4\varepsilon \left\{ \left(\frac{\sigma - 2a}{r_{ij} - 2a} \right)^{12} - \left(\frac{\sigma - 2a}{r_{ij} - 2a} \right)^{6} \right\} \tag{9}$$

where ε is the well depth, σ is the value of r where $\varphi(r)$ crosses zero, a is the radius of the hard core, and r_{ij} is the intermolecular separation between molecule i and molecule j. Figure 3 compares the HCLJ potential with the HCSW potential model. The HCLJ model has a repulsive hard core with radius a; however, the potential approaches infinity asymptotically. The attractive well region has the realistic parabolic shape, and at large separations, the potential is attractive approaching zero asymptotically as r goes to infinity. The HCLJ model is a much more realistic representation of the actual intermolecular potential than the HCSW model.

We fit the HCLJ potential parameters to the HBr and BCl_3 data, in the same way that Trusler used the Maitland–Smith potential [13] with his propane data [14]. For each intermolecular potential, we calculated the classical second and third virial coefficients and their temperature derivatives [15, 16]. The calculation of the third virial coefficient requires inclusion of three-body contributions. This adds an additional adjustable parameter. Like Trusler [14], we used the Axilrod–Teller triple–dipole term [17]:

$$\varphi(r_{123}) = \frac{\nu_{123}(1 + \cos\theta_1 \cos\theta_2 \cos\theta_3)}{(r_{12}^3 r_{13}^3 r_{23}^3)} \tag{10}$$

where ν_{123} is the dispersion coefficient, and θ_i is defined as the angle subtended at molecule i by molecules j and k. This is the first term in the three-body corrections to the dispersion energy for monatomic species. The integral equations providing the second and third virial coefficients for spherically symmetric molecules are given by

$$B(T) = -2\pi N_A \int_0^\infty f_{12} r_{12}^2 \, dr_{12} \tag{11}$$

$$C(T) = -\frac{8\pi^2 N_A^2}{3} \int_0^\infty \int_0^\infty \int_{|r_{12} - r_{13}|}^{|r_{12} + r_{13}|} (f_{12} f_{13} f_{23} - e_{12} e_{13} e_{23} f_{123}) \times r_{12} r_{13} r_{23} \, dr_{12} \, dr_{13} \, dr_{23} \tag{12}$$

where r_{ij} is the distance between molecule i and molecule j, $e_{ij} = \exp\{-\varphi(r_{ij})/kT\}$, $f_{ij} = e_{ij} - 1$, and $f_{ijk} = \exp\{-\varphi(r_{ijk})/kT\} - 1$. Equations (11) and (12) allow us to calculate the second and third virial coefficients and their temperature derivatives for a given intermolecular potential at a given temperature. With $C_p^o(T)/R$ given by Eqs. (2) and (3), only four potential parameters, ε, σ, a, and v_{123} are required to fit the $u^2(T, P)$ surface. Initial guesses of ε, σ, and a were determined by fitting the HCLJ second virial coefficient to that determined with the HCSW model. These parameters were fixed and an initial value for v_{123} was determined by fitting only v_{123} to the values of the third virial coefficient determined from the HCSW method. Then all four parameters were varied while fitting to the $u^2(T, P)$ surface. The resulting parameters are given in Table V.

5.2.1. The HCLJ Model for HBr

Figure 4 (bottom) shows the deviations of the measured speeds of sound from those predicted from the presented HCLJ equation of state. The fit had 225 degrees of freedom, v, and $\chi^2/v = 0.74$. The HCLJ model has two fewer fitting parameters than the HCSW model. The HCLJ model reproduced the measured speeds of sound with a relative standard deviation of 0.004%, essentially the same as that of the six-parameter HCSW model.

5.2.2. The HCLJ Model for BCl_3

As in the case of the HCSW model, each high-pressure isotherm was adjusted by the fixed parameter f_c as reported in Table II. Figure 5 (bottom) shows the deviations of the $u(T, P)$ values from those calculated from the present HCLJ equation of state. The fit of the HCLJ model to the BCl_3 data had 162 degrees of freedom, v, and $\chi^2/v = 4.71$. The equation of state reproduced the measured and adjusted speeds of sound with a relative standard deviation of 0.003%, and the unadjusted speeds of sound with a relative standard deviation of 0.010%. The high precision of our data allows trends in the deviations of each isotherm to be seen in Fig. 5. The most likely source of these trends is our fitting a planar molecule to a spherically symmetric potential. This may indicate that further modeling may have to take anisotropy into account.

Table V. Hard-Core Lennard–Jones Potential Parameters

	σ (nm)	ε/k_B (K)	a (nm)	v_{123}/k_B (K · nm^9)
HBr	0.34397	533.45	0.056232	0.004286340
BCl_3	0.49963	621.72	0.087456	0.056453407

5.2.3. Interpolation Scheme

The computation of the second and third virial coefficients and their temperature derivatives from Eqs. (11) and (12) using the parameters in Table V is a numerically intensive process and is not convenient for repetitive calculations. Again, following the lead of Trusler [14], we provide a look-up table for the second and third virial coefficients and their first two derivatives, along with a preferred method of interpolation. In the look-up table, a substitution of variables has been performed, such that temperature is presented as reduced reciprocal temperature $\tau = e/kT$, where $T(dB/dT) = -\tau(dB/d\tau)$ and $T^2(d^2B/dT^2) = \tau^2(d^2B/d\tau^2) + 2\tau(dB/d\tau)$. In Tables VI and VII the virial coefficients are also presented in reduced (unitless) form where $B^*(T) = B(T)/b_o$ and $C^*(T) = C(T)/b_o^2$, where $b_o = 2\pi N_A\sigma^3/3$. Tables VI and VII provide reduced temperatures between 0.3 and 3.0, which corresponds to approximately 178 to 1780 K for HBr and 233 to 2330 K for BCl_3. These ranges greatly exceed our experimental temperature ranges; however, they are reasonable extrapolations based on our experience with CF_4 and C_2F_6 and Trusler's experience with C_3H_8. The recommended interpolation of $B^*(\tau)$, $C^*(\tau)$ or their derivatives at τ between adjacent points at τ_1 and τ_2 is the cubic polynomial $f(\tau)$ such that

$$f(\tau) = a(\tau-\tau_1) + b(\tau-\tau_2) + \{c(\tau-\tau_1) + d(\tau-\tau_2)\}(\tau-\tau_1)(\tau-\tau_2)$$
$$a = f(\tau_2)/\Delta\tau, \qquad c = \{f'(\tau_2)/(\Delta\tau)^2\} - \{(a+b)/(\Delta\tau)^2\} \tag{15}$$
$$b = -f(\tau_1)/\Delta\tau, \qquad d = \{f'(\tau_1)/(\Delta\tau)^2\} - \{(a+b)/(\Delta\tau)^2\}$$

where $f' = df/d\tau$ and $\Delta\tau = \tau_2 - \tau_1$. To allow the calculation of the second derivatives, the third derivatives are included in Tables VI and VII.

5.3. Equation-of-State Estimation Methods

No previously published second or third virial coefficients could be found in the literature for either HBr or BCl_3. This work is the first to measure the nonidealities of these important compounds. This will be the case for many of the species we plan to study in the future. However, empirical correlations are available for estimating virial coefficients. Weber [18] adapted the correlations of Pitzer and Curl [19], Tsonopolulos [20], and Kohler and co-workers [21, 22] to estimate the second and third virial coefficients of small polar molecules. Figure 6 compares our results for the HCLJ model with Weber's correlation. In general, the Weber correlation does surprisingly well. When compared to our equation of state for HBR, gas densities calculated from Weber's correlation differ from our HCLJ

Table VI. HBr Reduced Virial Coefficients and Their Derivatives with Reduced Temperature

τ	$B(\tau^*)$	$\frac{\partial B(\tau)^*}{\partial \tau}$	$\frac{\partial^2 B(\tau)^*}{\partial \tau^2}$	$\frac{\partial^3 B(\tau)^*}{\partial \tau^3}$	$C(\tau)^*$	$\frac{\partial C(\tau)^*}{\partial \tau}$	$\frac{\partial^2 C(\tau)^*}{\partial \tau^2}$	$\frac{\partial^3 C(\tau)^*}{\partial \tau^3}$
0.3	0.04213	−0.14826	−0.17639	0.55279	0.00398	0.00099	0.01017	0.09644
0.4	0.02649	−0.16394	−0.14334	0.17901	0.00415	0.00239	0.01712	0.05033
0.5	0.00940	−0.17766	−0.13314	0.04424	0.00448	0.00431	0.02104	0.03000
0.6	−0.00902	−0.19087	−0.13218	−0.01828	0.00502	0.00654	0.02333	0.01611
0.7	−0.02878	−0.20424	−0.13591	−0.05359	0.00579	0.00894	0.02427	0.00247
0.8	−0.04989	−0.21815	−0.14252	−0.07721	0.00681	0.01135	0.02373	−0.01399
0.9	−0.07243	−0.23282	−0.15118	−0.09545	0.00806	0.01362	0.02130	−0.03557
1.0	−0.09648	−0.24844	−0.16152	−0.11123	0.00952	0.01553	0.01636	−0.06464
1.1	−0.12215	−0.26517	−0.17339	−0.12605	0.01114	0.01678	0.00803	−0.10394
1.2	−0.14956	−0.28317	−0.18673	−0.14075	0.01284	0.01698	−0.00488	−0.15692
1.3	−0.17883	−0.30257	−0.20156	−0.15587	0.01448	0.01560	−0.02395	−0.22800
1.4	−0.21013	−0.32353	−0.21793	−0.17176	0.01588	0.01191	−0.05127	−0.32285
1.5	−0.24360	−0.34621	−0.23594	−0.18870	0.01676	0.00498	−0.08956	−0.44882
1.6	−0.27943	−0.37078	−0.25571	−0.20693	0.01673	−0.00648	−0.14238	−0.61538
1.7	−0.31782	−0.39741	−0.27738	−0.22665	0.01526	−0.02414	−0.21439	−0.83484
1.8	−0.35899	−0.42632	−0.30110	−0.24807	0.01162	−0.05020	−0.31164	−1.12309
1.9	−0.40317	−0.45771	−0.32706	−0.27139	0.00484	−0.08757	−0.44198	−1.50069
2.0	−0.45062	−0.49181	−0.35545	−0.29683	−0.00639	−0.14004	−0.61563	−1.99425
2.1	−0.50163	−0.52889	−0.38650	−0.32461	−0.02383	−0.21257	−0.84583	−2.63816
2.2	−0.55651	−0.56921	−0.42046	−0.35498	−0.04979	−0.31165	−1.14975	−3.47690
2.3	−0.61559	−0.61308	−0.45759	−0.38819	−0.08733	−0.44571	−1.54961	−4.56797
2.4	−0.67925	−0.66084	−0.49820	−0.42454	−0.14046	−0.62572	−2.07421	−5.98574
2.5	−0.74790	−0.71285	−0.54261	−0.46434	−0.21447	−0.86594	−2.76082	−7.82634
2.6	−0.82198	−0.76950	−0.59119	−0.50792	−0.31627	−1.18488	−3.65767	−10.21412
2.7	−0.90197	−0.83124	−0.64433	−0.55565	−0.45487	−1.60655	−4.82719	−13.30987
2.8	−0.98841	−0.89854	−0.70247	−0.60795	−0.64203	−2.16207	−6.35011	−17.32161
2.9	−1.08188	−0.97192	−0.76609	−0.66527	−0.89307	−2.89180	−8.33093	−22.51851
3.0	−1.18302	−1.05196	−0.83571	−0.72808	−1.22792	−3.84798	−10.90482	−29.24890

Table VII. Boron Trichloride Reduced Virial Coefficients and Their Derivatives with Reduced Temperature

τ	$B(\tau)^*$	$\frac{\partial B(\tau)^*}{\partial \tau}$	$\frac{\partial^2 B(\tau)^*}{\partial \tau^2}$	$\frac{\partial^3 B(\tau)^*}{\partial \tau^3}$	$C(\tau)^*$	$\frac{\partial C(\tau)^*}{\partial \tau}$	$\frac{\partial^2 C(\tau)^*}{\partial \tau^2}$	$\frac{\partial^3 C(\tau)^*}{\partial \tau^3}$
0.3	0.04480	−0.14065	−0.16995	0.53779	0.00361	−0.00084	0.00670	0.08855
0.4	0.02995	−0.15574	−0.13776	0.17465	0.00358	0.00018	0.01291	0.04323
0.5	0.01371	−0.16891	−0.12777	0.04386	0.00366	0.00164	0.01612	0.02272
0.6	−0.00381	−0.18158	−0.12675	−0.01674	0.00391	0.00335	0.01765	0.00824
0.7	−0.02261	−0.19441	−0.13026	−0.05091	0.00434	0.00513	0.01776	−0.00628
0.8	−0.04271	−0.20773	−0.13656	−0.07372	0.00494	0.00684	0.01629	−0.02386
0.9	−0.06418	−0.22178	−0.14484	−0.09131	0.00570	0.00832	0.01281	−0.04682
1.0	−0.08710	−0.23675	−0.15474	−0.10651	0.00658	0.00932	0.00667	−0.07757
1.1	−0.11156	−0.25278	−0.16611	−0.12076	0.00753	0.00953	−0.00306	−0.11894
1.2	−0.13769	−0.27002	−0.17889	−0.13489	0.00845	0.00855	−0.01759	−0.17448
1.3	−0.16561	−0.28861	−0.19310	−0.14940	0.00919	0.00580	−0.03858	−0.24877
1.4	−0.19546	−0.30869	−0.20879	−0.16466	0.00953	0.00055	−0.06816	−0.34767
1.5	−0.22740	−0.33042	−0.22606	−0.18092	0.00918	−0.00821	−0.10918	−0.47883
1.6	−0.26161	−0.35396	−0.24502	−0.19841	0.00773	−0.02179	−0.16533	−0.65213
1.7	−0.29826	−0.37948	−0.26579	−0.21734	0.00460	−0.04194	−0.24144	−0.88040
1.8	−0.33758	−0.40718	−0.28854	−0.23789	−0.00096	−0.07095	−0.34379	−1.18029
1.9	−0.37978	−0.43726	−0.31343	−0.26027	−0.00998	−0.11185	−0.48060	−1.57339
2.0	−0.42511	−0.46995	−0.34066	−0.28468	−0.02385	−0.16857	−0.66250	−2.08769
2.1	−0.47386	−0.50548	−0.37044	−0.31134	−0.04440	−0.24631	−0.90337	−2.75950
2.2	−0.52631	−0.54413	−0.40301	−0.34048	−0.07404	−0.35181	−1.22121	−3.63593
2.3	−0.58280	−0.58618	−0.43863	−0.37235	−0.11597	−0.49389	−1.63939	−4.77804
2.4	−0.64367	−0.63196	−0.47758	−0.40723	−0.17441	−0.68403	−2.18829	−6.26507
2.5	−0.70933	−0.68182	−0.52019	−0.44542	−0.25488	−0.93720	−2.90730	−8.19980
2.6	−0.78019	−0.73613	−0.56679	−0.48723	−0.36460	−1.27285	−3.84757	−10.71559
2.7	−0.85672	−0.79532	−0.61777	−0.53304	−0.51303	−1.71628	−5.07550	−13.98555
2.8	−0.93943	−0.85985	−0.67354	−0.58323	−0.71253	−2.30038	−6.67724	−18.23438
2.9	−1.02888	−0.93021	−0.73457	−0.63823	−0.97921	−3.06788	−8.76463	−23.75391
3.0	−1.12568	−1.00695	−0.80136	−0.69851	−1.33405	−4.07429	−11.48288	−30.92318

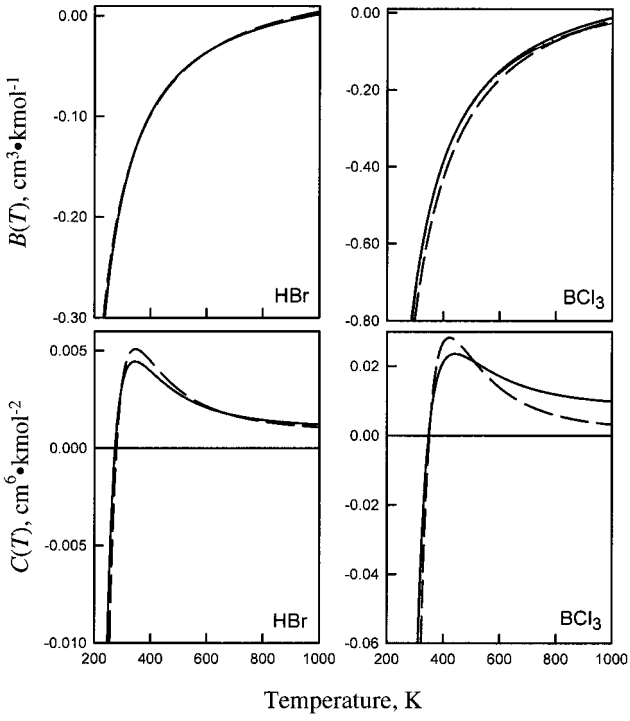

Fig. 6. Second and third virial coefficients. (——) HCLJ equation of state; (- - - - -) predicted values by Ref. 18.

model by less than 1% up to densities of 3000 $mol \cdot m^{-3}$. Weber's correlation for BCl_3 agrees with our equation of state for BCl_3 to within 1% only up to gas densities of 200 $mol \cdot m^{-3}$. Boron trichloride is not a polar molecule; in the Weber correlation its dipole moment is set to zero.

6. TRANSPORT PROPERTIES

The process of fitting the parameters of the HCLJ intermolecular potential to the $u^2(T, P)$ surface results in an effective, spherically symmetric, intermolecular potential, which is an average over all collision orientations. It is known that fitting the nonidealities of a gas is not sufficient to determine the unique intermolecular potential for a species and that the HCLJ model is not the correct shape of the intermolecular potential and that these molecules are not spherically symmetric. Nevertheless, ideal-gas viscosities (η^o) and thermal conductivities (λ^o) calculated from these approximate intermolecular potentials can be quite useful [23]. The

viscosities for CF_4, C_2F_6, C_3H_8, and SF_6 calculated from intermolecular potentials fitted to speed-of-sound measurements agree with the experimental values of viscosity to better than 10%. In the case of SF_6 the calculated viscosities were, on average, 4% below the experimental values. The viscosities estimated from the HCLJ potential determined for CF_4 and C_2F_6 from the $u(T, P)$ measurements were, on average, 5% below the measured viscosities. Similarly, the viscosity of propane predicted by Trusler's Maitland–Smith intermolecular potential fitted to his $u(T, P)$ data deviates from measured viscosity values by +4.2% at 200 K, −1.6% at 300 K, and −6.5% at 500 K [14].

Figure 7 shows the dilute gas viscosities estimated for HBr and BCl_3 from the presented HCLJ potentials together with other published viscosity estimates. There are no published measurements of the viscosity of HBr or BCl_3 to compare with our estimates. Included in Fig. 7 is a published [6] estimate of the viscosity of SF_6 that was obtained using the same procedures used here. The deviations of the SF_6 data [27–29] from our estimates indicate the size of the deviations that one might obtain when the viscosities of HBr and BCl_3 are measured.

The viscosities estimated for HBr and BCl_3 from the HCLJ potentials were fitted by the empirical function.

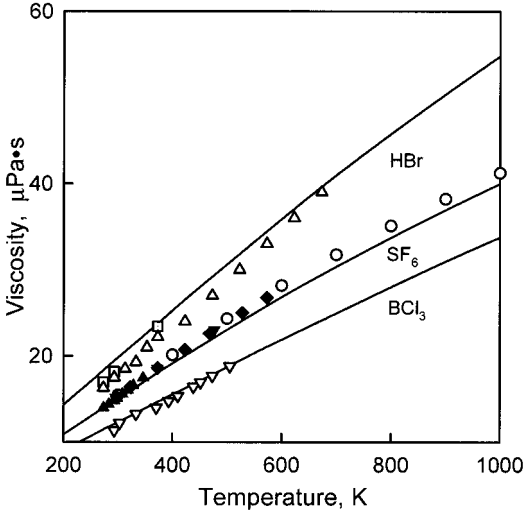

Fig. 7. Ideal-gas viscosities. Curves and open symbols are estimates; solid symbols are measurements. (——) Present estimate. HBr: (□) Ref. 24; (△) Ref. 25. BCl_3: (▽) Ref. 25. SF_6: (○) Ref. 26; (◆) Ref. 27; (▲) Ref. 28; (▼) Ref. 29.

$$\text{HBr:}\quad \ln\left(\frac{\eta^o}{\mu\ \text{Pa}\cdot\text{s}}\right) = -2.976 + 50.33\left(\frac{\text{K}}{T}\right) + 1.0172\ln\left(\frac{T}{\text{K}}\right) - 9.885\text{E-}08\left(\frac{T}{\text{K}}\right)^2 \tag{15a}$$

$$BCl_3\text{:}\quad \ln\left(\frac{\eta^o}{\mu\ \text{Pa}\cdot\text{s}}\right) = -3.567 + 70.98\left(\frac{\text{K}}{T}\right) + 1.0251\ln\left(\frac{T}{\text{K}}\right) - 6.638\text{E-}08\left(\frac{T}{\text{K}}\right)^2 \tag{15b}$$

Equations (15a) and (15b) represent the calculated viscosities to within 0.1% of η^o. We expect that the calculated ideal-gas viscosities are within 10% of their true values throughout the temperature range of 200 K $\leqslant T \leqslant$ 1000 K for HBr and 280 K $\leqslant T \leqslant$ 1000 K for BCl_3.

The ideal-gas thermal conductivity of dilute gases can be estimated from the viscosity and the constant-volume ideal-gas heat capacity with the Eucken [30] approximation,

$$[\lambda^o]_{\text{Eucken}} = \frac{15}{4}\frac{R}{M}\eta^o\left(\frac{4}{15}\frac{C_v^\circ}{R} + \frac{3}{5}\right) \tag{17}$$

We have calculated λ^o from Eq. (15) using Eqs. (2) and (16) and values of C_p° from the JANAF [31] tables. The following simple polynomial was fitted to the resulting values of λ^o:

$$\text{HBr:}\quad \ln\left(\frac{\lambda^o}{\text{W}\cdot\text{m}^{-1}\cdot\text{K}^{-1}}\right) = -10.835 + 64.61\left(\frac{\text{K}}{T}\right) + 1.0484\ln\left(\frac{T}{\text{K}}\right) - 1.592\text{E-}08\left(\frac{T}{\text{K}}\right)^2 \tag{17a}$$

$$BCl_3\text{:}\quad \ln\left(\frac{\lambda^o}{\text{W}\cdot\text{m}^{-1}\cdot\text{K}^{-1}}\right) = -10.580 - 31.35\left(\frac{\text{K}}{T}\right) + 1.0204\ln\left(\frac{T}{\text{K}}\right) - 8.838\text{E-}08\left(\frac{T}{\text{K}}\right)^2 \tag{17b}$$

Equations (17a) and (17b) represent the calculated values of λ^o to 0.1% standard relative uncertainty. The values of λ^o from Eqs. (17a) and (17b) have relative standard uncertainties of the order of 10%. They come from the relative standard uncertainty of the viscosity ($\approx$5%), the Eucken approximation ($\approx$10%) [32], and C_v ($\approx$1%). In future work, we will

use an acoustic technique to measure the thermal conductivity and the viscosity [33]. This will allow us to test our transport property estimates. Also in future work, we will examine mixtures of process gases with carrier gases such as argon, helium, and nitrogen. In these cases it will be necessary to fit the interaction potentials, from which we will estimate the diffusion coefficient. Diffusion coefficients are required to model processes where the rate-limiting step is the diffusion of a reactant from a carrier gas to a hot silicon surface.

ACKNOWLEDGMENT

This work was supported in part by the The National Semiconductor Metrology Program, managed by the Office of Microelectronics Programs, an office within NIST.

REFERENCES

1. A. R. H. Goodwin and M. R. Moldover, *J. Chem. Phys.* **95**:5236 (1991).
2. K. A. Gillis, *Int. J. Thermophys.* **18**:73 (1997).
3. J. J. Hurly, *Int. J. Thermophys.* **20**:455 (1999).
4. K. A. Gillis, *Int. J. Thermophys.* **15**:821 (1994).
5. K. A. Gillis, A. R. H. Goodwin, and M. R. Moldover, *Rev. Sci. Instrum.* **62**:2213 (1991).
6. J. J. Hurly, submitted for publication (1999).
7. D. R. Stull, *Ind. Eng. Chem.* **39**:517 (1947).
8. J. F. Mathews, *Chem. Rev.* **72**:71 (1972).
9. R. E. Lynn, Jr. and K. A. Kobe, *Chem. Rev.* **52**:117 (1953).
10. J. E. Mayer and M. G. Mayer, *Statistical Mechanics* (John Wiley & Sons, New York, 1959), p. 469.
11. K. A. Gillis and M. R. Moldover, *Int. J. Thermophys.* **17**:1305 (1996).
12. T. Kihara, *Rev. Mod. Phys.* **25**:831 (1953).
13. C. G. Maitland and E. B. Smith, *Chem. Phys. Lett.* **22**:443 (1973).
14. J. P. M. Trusler, *Int. J. Thermophys.* **18**:635 (1997).
15. E. A. Mason and T. H. Spurling, *The Virial Equation of State* (Pergamaon Press, Oxford, 1969).
16. R. J. Dulla, J. S. Rowlinson, and W. R. Smith, *Mol. Phys.* **21**:229 (1971).
17. B. M. Axilrod and E. J. Teller, *J. Chem. Phys.* **11**:299 (1943).
18. L. A. Weber, *Int. J. Thermophys.* **15**:461 (1994).
19. K. S. Pitzer and R. F. Curl, Jr., *J. Am. Chem. Soc.* **79**:2369 (1957).
20. Tsonopolulos, *AIChE J.* **24**:1112 (1978).
21. N. Van Nhu, G. A. Iglesias-Silva, and F. Kohler, *Ber. Bunsenges. Phys. Chem.* **93**:526 (1989).
22. N. Van Nhu and F. Kohler, *Ber Bunsenges Phys. Chem.* **92**:1129 (1988).
23. J. O. Hirschfelder, C. F. Curtiss, and R. B. Bird, *Molecular Theory of Gases and Liquids* (John Wiley & Sons, New York, 1954).
24. A. E. Schuil, *Phil. Mag.* **28**:679 (1939).
25. *Matheson Gas Data Book*, unabridged ed. (Matheson Company, East Rutherford, NJ, 1974).

26. R. A. Suehla, *NASA-TR-R*-132 **116**:57, 79 (1962).
27. T. S. Ro, J. Kestin, and J. M. Hellemans, *Physica* **65** (1973).
28. K. Veda and K. Kigoshi, *J. Inorg. Nucl. Chem.* **36**:989 (1974).
29. W. A. Wakeham, H. E. Khalifa, and J. K. Esti, *J. Chem. Phys.* **65**:5186 (1976).
30. A. Eucken, *Phys. Z.* **14**:324 (1913).
31. *JANAF Thermochemical Tables*, 2nd ed., NSRDS-NBS 37 (U.S. Department of Commerce, Washington, DC, 1971).
32. R. C. Reid, J. M. Prausnitz, and T. K. Sherwood, *The Properties of Gases and Liquids*, 3rd ed. (McGraw–Hill, New York, 1977).
33. K. A. Gillis, J. B. Mehl, and M. R. Moldover, *Rev. Sci. Instrum.* **67**:1850 (1996).
34. *BYU DIPPR801 Thermophysical Properties Database*, Spring 1998 Preview Release (Brigham Young University, Provo, UT 84602).
35. E. W. Lemmon, M. O. McLinden, and D. G. Friend, in *NIST Chemistry WebBook*, NIST Standard Reference Database Number 69, W. G. Mallard and P. J. Linstrom, eds. (National Institute of Standards and Technology, Gaithersburg, MD, Nov. 1998) (http://webbook.nist.gov).
36. B. J. McBride, S. Gordon, and M. A. Reno, *Coefficients for Calculating Thermodynamic and Transport Properties of Individual Species*, NASA Report TM-8209 4513 (1993).
37. E. F. Westrum, D. R. Stull, and G. C. Sinke, *The Chemical Thermodynamics of Organic Compounds* (John Wiley and Sons, New York, 1969).
38. A. R. Gordon and C. Barnes, *J. Chem. Phys.* **1**:692 (1933).
39. E. G. Long and K. A. Kobe, *Petrol. Refin.* **29:**124 (1950).
40. J. B. Austin, *J. Am. Chem. Soc.* **54**:3459 (1932).
41. *JANAF Thermochemical Tables*, 3rd ed., *J. Phys. Chem. Ref. Data Suppl.* **1**:14 (1985).
42. *Thermodynamic Properties of Individual Substances*, 4th ed., *Vol 2. Elements Carbon, Silicon, Germanium, Tin, Lead, and Their Compounds, Pt. 2. Tables* (Hemisphere, New York, 1991).
43. D. Wagman, R. Schumm, V. Parker, R. Nuttall, I. Halow, W. Evans, K. Churney, and S. Bailey, *J. Phys. Chem. Ref. Data Suppl.* **2** (1982).
44. D. R. Lide (ed.), *Handbook of Chemistry and Physics*, 75th ed. (CRC Press, Boca Raton, FL, 1994).